Applied Current Thermoacoustic Imaging

Yanju Yang[1,2], Yanhong Li[1,2], Zhengwu Xia[1], Yuanyuan Li[1,2], Wenxiu Sun[1,2], and Guoqiang Liu[1,2*]

[1]Institute of Electrical Engineering, Chinese Academy of Sciences, Beijing, 100190 China
[2]University of Chinese Academy of Sciences, Beijing, 100190 China
*Corresponding author e-mail: liuguoqiang@mail.iee.ac.cn

Applied Current Thermoacoustic Imaging (ACTAI) is exploited theoretically and demonstrated in gel phantom studies. In ACTAI, a microsecond width pulse current is applied to an object, which emits thermoacoustic waves after absorbing the Joule heating. The thermoacoustic signals are acquired by acoustic transducers to reflect conductivity distribution of the object. This approach with MHz pulse electric can extend thermoacoutic imaging to deep biological tissues. In this paper, the formulas of forward and inverse problems in ACTAI are deduced. Numerical simulation and experimental study on low conductivity phantoms are conducted. The results provide foundations of studies on biological tissues for ACTAI.

***Index Terms*—Biomedical imaging, Electromagnetic analysis, Eddy currents, Thermal expansion**

I. Introduction

IN THE PAST decades, researchers have suggested that using thermoacoustic effect[1]-[3]can be a powerful imaging technology with high spatial resolution of ultrasonography and large dielectric contrast of tissues. To explore a potential deeper penetration and more energy efficient method, Zheng et al investigated theoretically the feasibility of applying magnetic field at radio frequency below 20MHz to heat conductive or magnetic nanoparticles objects for mediating thermoacoustic imaging, which is Magnetically Mediated Thermoacoustic Imaging (MMTAI)[4]-[5]. This approach is promising to adopt low frequency magnetic field for achieving thermoacoustic imaging, which is proved by the preliminary numerical and experimental results. Here, we report a different approach called Applied Current Thermoacoustic Imaging (ACTAI) that applies pulsed electric field with microsecond pulse current injection to the biological tissue for thermoacoustic generation, which depends on Joule heating for the thermodynamic equilibrium of the tissue and causes to thermoacoustc wave emission.

II. Theory

In this section, the formulas for the forward and inverse problem in ACTAI are derived.

The conceptual framework of ACTAI is shown in Fig.1. The object is injected an approximate microsecond pulse current, which creates a pulsed electric field $E(r',t)$ inside it, where r' denotes the position inside the object. The areas of A and B are injected current with the electrodes. The electric potential of A is $U(t)$ and B is 0, respectively. The conductivity of the object is $\sigma(r')$.

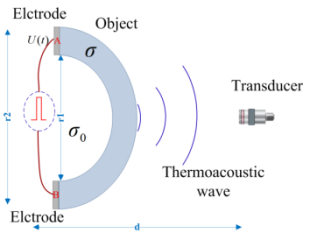

Fig. 1. Generation and propagation process of signals in ACTAI.

The equations governing the boundary problem of the electro quasi-static field can be described as follows

$$\begin{cases} \nabla\cdot(\sigma\nabla\phi)=0 \\ \phi|_A = U(t) \\ \phi|_B = 0 \\ \left.\dfrac{\partial\phi}{\partial n}\right|_{\Gamma\setminus A\setminus B}=0 \end{cases} . \quad (1)$$

where ϕ is the electric scalar potential and Γ is the outer boundary of the object. The electric scalar potential can be calculated by solving Eq.(1). According to Helmholtz theorem, electric field can be expressed as $\boldsymbol{E}(r',t)=-\nabla\phi$. Then the current density distribution $\boldsymbol{J}(r',t)=\sigma\boldsymbol{E}(r',t)$ flowing in the object, leads to absorption of joule heating. The heating function $Q(r',t)$ is expressed as the product of a spatial absorption function $Q(r')$ and a temporal illumination function $I(t)$, which is $Q(r',t)=Q(r')I(t)$. The spatial absorption function is $Q(r')=\sigma|E(r')|^2$. After the object absorbs joule heating, acoustic signal is generated due to the transient thermal expansion. The wave equation of ACTAI is

$$\nabla^2 p(r,t)-\frac{1}{c_s^2}\frac{\partial^2}{\partial t^2}p(r,t)=-\frac{\beta}{C_P}\frac{\partial Q(r',t)}{\partial t}=-\frac{\beta}{C_P}Q(r')\frac{\partial I(t)}{\partial t}. \quad (2)$$

where c_s, C_p β denotes the acoustic velocity, specific heat capacity, isobaric volume expansion coefficient of the object, and $p(r,t)$ is the acoustic pressure at the position $\boldsymbol{r}$ of the transducer. The $p(r,t)$ can be solved by Green's function [6] as

$$p(r,t)=\frac{1}{4\pi}\iiint_{\Omega}\frac{\beta}{C_P}\frac{\partial Q(r',t)}{\partial t}\frac{\delta(t-|\boldsymbol{r}'-\boldsymbol{r}|/c_s)}{|\boldsymbol{r}'-\boldsymbol{r}|}dr'. \quad (3)$$

where Ω is the whole area of the integration which contains all the acoustic sources, respectively. According to Eq.(2), it provides the basic formula to calculate the acoustic pressure with the given electric field within and near the object.

The inverse problem of ACTAI is to study how to reconstruct the acoustic source distribution using the collected acoustic signal, either simulated or experimented. The source term of the wave equation can be reconstructed by the time reversal algorithm, as

$$Q(r')\approx\frac{C_P}{2\pi c_s^3\beta}\oint_{\Sigma}dS\,\frac{\boldsymbol{n}\cdot\boldsymbol{e_R}}{R}\frac{\partial p(r',|r'-r|/c_s)}{\partial t}. \quad (4)$$

III. Simulation Study

To demonstrate the validity and reliability of the presented theories of ACTAI, a 2-D simulation was carried out with a low conductivity semi-circular ring model to calculate the pressure $p(r,t)$ by finite element method. The conductivity of the semi-circular ring model is set to 1S/m. The inner and outer radius of the object is set to 0.03m and 0.05m, respectively. In order to couple acoustic, the transducer and the model are immersed into insulation oil, whose conductivity is 0 S/m. The acoustic velocity in the oil is set to 1400 m/s. The acoustic system in this paper is set to be uniform not to think about any acoustic dispersion, attenuation and reflection. The function of the voltage added to the object is$U(t) = 100\mathrm{e}^{-(\mathrm{t}-\mathrm{b})^2/2\mathrm{c}^2}$, where b=5×10^{-7}and c=1×10^{-7}. The center frequency of the transducer is 1MHz.

During simulations, the norm of the electric field strength at t=0.5us is shown as Figure 2(a). The normalized waveform detected by the transducer at the point (0.03, 0) m is shown in Figure 2(b). The wave cluster begins at 0.01m and ends at 0.05m, which coincide with the propagation distance of the acoustic wave corresponding to the outer and inner edge of the model to the transducer. The later cluster has higher amplitude because of the electric field norm of the inner medium.

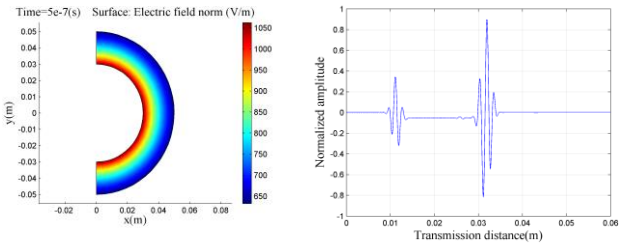

(a) (b)

Fig. 2. Simulation results of the ACTAI. (a) The norm of the electric field strength. (b) Waveform detected by the transducer.

IV. Experiments

ACTAI experiment has been conducted using a gel phantom to check the feasibility of this method. In the setup, the insulation oil was placed in a plastic tank to a certain height in order to immerse the object and the transducer for coupling acoustic wave. A signal generator and an amplifier form the current excitation, which adds a microsecond pulse current to the object. The amplitude of voltage added to the object is 100V. The object is mounted well on a stage and maintains the same horizontal level with the center axis of transducer. The acoustic signals detected by the transducer (A303S, Olympus) are amplified by an amplifier (5058R, Olympus), and then are displayed and recorded by an oscilloscope (DSO7052A, Agilent) for processing.

The semi-circular ring phantom was made of 20% cooled salinity gel with a thickness of 1mm. Its inner and outer diameter is 0.03m and 0.055m respectively. The distance between the center of the phantom and the interface of the transducer is set to be 14cm. The experiment diagram is shown as Fig.3(a). The acoustic signal waveform obtained by an oscillography is shown in Fig.3(b). CH2 is the acoustic pressure (2mV/div) detected by the transducer. There are two wave clusters of the conductivity boundaries at about 58μs and 66μs, which match the distances from the point of the transducer to the outer and the inner boundary of the ring model, agreeing with the acoustic wave propagation delay. This proves that the signal is caused by the two boundaries of the semi-circular ring gel phantom, and it shows the position of conductivity changes of the object. The transducer was installed on a mechanical scanning device, and was scanned around the object in a half circle trajectory for data acquisition to reconstruct acoustic source by time reversal algorithm. The reconstructed image is shown in Fig.3.(c). The reconstruction image represents the shape and size of the phantom and it can reflect the conductivity distribution changes of the object.

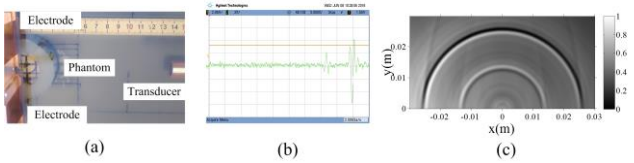

(a) (b) (c)

Fig. 3. Experiment diagram of ACTAI. (a) The experimental setup. (b) The acoustic signal detected by the transducer. (c) The reconstructed image.

V. Conclusion

In conclusion, a study was performed on ACTA. In the theoretical section, the formulae for the acoustic signals of ACTAI have been provided based on the theories of electromagnetic fields, thermal expansion and acoustic detection. A numerical simulation and an experiment setup on low conductivity similar to the biological tissues have been investigated. The numerical simulation and the salinity gel phantom experiment demonstrate the validity of the proposed method. The results of this study offer a new imaging method for early disease diagnosis to deeper penetration.

Acknowledgments

Research supported by the National Natural Science Foundation of China under Grant Nos 51137004, 51477161 and 61427806.

References

[1] Z. Liu, L. Liu, Y. Xu, et al, "Transcranial thermoacoustic tomography: a comparison of two imaging algorithms," *IEEE Trans. Med. Imaging.* vol.32, pp. 289-294. 2012.

[2] T. Qin, X. Wang, Y. Qin, et al, "Experimental Validation of a Numerical Model for Thermoacoustic Imaging Applications," *IEEE Antennas Wireless Propag. Lett.* vol.14, pp. 1235-1238. 2015.

[3] X. Wang, T. Qin, R. S. Witte, et al, "Computational Feasibility Study of Contrast-Enhanced Thermoacoustic Imaging for Breast Cancer Detection Using Realistic Numerical Breast Phantoms," *IEEE Trans. Microw. Theory Tech.* vol.63, pp. 1-13. 2015.

[4] X. H. Feng, F. Gao and Y. J. Zheng, "Magnetically mediated thermoacoustic imaging toward deeper penetration," *Appl. Phys. Lett.* vol.103, pp. 083704-083707. 2013.

[5] X. H. Feng, F. Gao and Y. J. Zheng, "Modulatable magnetically mediated thermoacoustic imaging with magnetic nanoparticles," *Appl. Phys. Lett.* vol.106, pp. 153702. 2015.

[6] G. Q. Liu, X. Huang, H. Xia, et al, "Magnetoacoustic tomography with current injection," *Chinese Sci. Bull.* vol.58, pp. 3600-3606. 2013.